coatings

MDPI

Article

Microstructural Evolution and Densification of Co-Based Alloy Powder by Spark Plasma Sintering for High-Hardness Applications

Fernando Juárez-López [1,*], Rubén Cuamatzi-Meléndez [1], Ángel de Jesús Morales-Ramírez [1,2], Margarita García-Hernández [3] and María Luz Carrera-Jota [2,4]

[1] Instituto Politécnico Nacional-CIITEC, Sta. Catarina, Azcapotzalco, Ciudad de México 02250, Mexico; ruben_c_m@yahoo.com.mx (R.C.-M.); amoralesra@ipn.mx (Á.d.J.M.-R.)
[2] Instituto Politécnico Nacional-ESIQIE, Lindavista, Gustavo A. Madero, Ciudad de México 07700, Mexico; mcarreraj@ipn.mx
[3] Instituto Politécnico Nacional-UPIIH, San Agustín Tlaxiaca 42162, Mexico; margaciah@ipn.mx
[4] Instituto Politécnico Nacional-ENCB, Nueva Industrial Vallejo, Gustavo A. Madero, Ciudad de México 07738, Mexico
* Correspondence: fjuarezl@ipn.mx

Abstract: This work presents the densification of Co-based alloy powders by a spark plasma sintering process. The densification process was carried out at a temperature range of 800 °C to 1100 °C in order to obtain sintered coupons and study their microstructure and mechanical properties. The shrinkage behaviour of the sintered coupons was studied, and an optimal densification temperature was defined. The microstructural analysis showed a reduction in porosity with temperature increment along with the development of a fine microstructure comprised of cobalt-molybdenum-chromium-silicon-based intermetallic laves phases, which are dispersed in a softer cobalt-based alloy matrix. X-diffraction analysis showed that these crystalline phases were well-dispersed, with a lattice parameter corresponding to a hexagonal system. The obtained high Vickers hardness values were attributed to the preservation of a fine microstructure and to the precipitation of Co-Mo phases. Three-point bending tests were performed in order to identify the strain path concerning the densification of the sintered coupons.

Keywords: spark plasma sintering; co-based alloy; densification; shrinkage

Citation: Juárez-López, F.; Cuamatzi-Meléndez, R.; Morales-Ramírez, Á.d.J.; García-Hernández, M.; Carrera-Jota, M.L. Microstructural Evolution and Densification of Co-Based Alloy Powder by Spark Plasma Sintering for High-Hardness Applications. *Coatings* **2024**, *14*, 479. https://doi.org/10.3390/coatings14040479

Academic Editors: Qi Hua Fan, Oleg Shichalin, Marcello Filgueira and Izabel Fernanda Machado

Received: 13 February 2024
Revised: 27 March 2024
Accepted: 11 April 2024
Published: 13 April 2024

1. Introduction

Co-based alloys have a unique resistance to corrosion and oxidation, excellent abrasive wear resistance properties, high temperature service, good hot hardness, and resistance to most harsh acidic and saline environments [1,2]. The above shows that cobalt alloys' characteristics can be beneficial to manufacturing of structural components for system aeronautics, prosthetic dentistry, and subsea production systems technologies, which are exposed to accelerated damage and subsequent failure of mechanical components [3–7].

The sintering spark plasma (SPS) process has extensively been used to densify metal powders placed in an electrically conducting die and sintered under a uniaxial load by heat produced using an electricity current arch [8,9]. Rapid heating by the Joule effect allows for short densification times, resulting in very efficient preservation of fine homogeneous microstructures. Moreover, the design of metastable or equilibrium microstructures can be performed or even controlled depending on the alloy and on the processing conditions. In the SPS process, the heat can increase from 100 °C to 240 °C in milliseconds, and rapid cooling/quenching rates of 200 °C/min can also be obtained, which are beneficial for densification processes [10]. Nonetheless, the densification process itself can modify the composition and structure of the material with some variations in the microstructure and mechanical properties.

The above shows that SPS is a process for manufacturing innovative materials with improved microstructures [11–15]. In this sense, the SPS process has demonstrated efficiency for shaping; nonetheless, it is empathized that the progress of shaping by SPS is complex. The full-scale parts and near-net shaping complex have been successfully proven, allowing for a wide range of possibilities, especially for materials that are difficult to obtain by conventional manufacturing processes [16]. However, it is worth noting that an understanding of the physical phenomena of the SPS process has been essential for the development of simulations of the kinetic densification, which has proven to be significant for optimizing the processing of complicated parts [17,18].

Thus, several research works have been performed to date by employing Co-based alloy powders and other cobalt alloys in SPS processes [19–21]. However, to our knowledge, there are no sintering studies concerning the composition of commercial Diamalloy powder, which consists of a cobalt-based alloy containing molybdenum, chromium, and silicon, where the higher molybdenum content in the powders increases its resistance, which is desirable in the development of metallic coatings [22,23]. Thus, it is expected that the SPS process improves the solubility of some chemical elements in the matrix by the formation of new phases.

Therefore, the aim of the present work was to study the sintering behaviour of a Co-based Diamalloy powder. Special attention was focused on the shrinkage rate and microstructural evolution of the mentioned powders in SPS conditions. Both Vickers hardness and three-point bending tests were performed in order to show how the sintering temperature variable plays an important role in the microstructure and mechanical properties. To determinate the microstructure, a JEOL-7800 high-resolution scanning electron microscope (Tokyo, Japan) with XL-EDAX Ametek-Apolo detector, windows of 30 mm, voltage of 10 Kv, and WD of 10–12 mm was used to characterize the sintered coupon. An X-ray diffraction (XRD) analysis of the sintered coupons was carried out with an X-ray diffractometer (Bruker D8-ECO Advance) with a Bragg–Brentano setup equipped with an X'Celeratrimina 2θ range of 20°–80° using a 0.021 step size, 2 s per step, and Cu-Ka radiation with l ¼ of 1.541 to determinate the crystalline structure.

2. Materials and Methods

Diamalloy 3001 commercial powders (SULZER Metco LT, Winterthur, Switzerland) comprised of a cobalt base with additions of Mo 28.5, Cr 17.5 and Si 3.4 wt.%, were used to manufacture shape coupons with a diameter of 20 mm and a thickness of 5 mm. A Dr Sinter Sumitomo 1050 apparatus (Sumitomo Coal Ming Co., Tokyo, Japan) was used to sinter 5 g of powder placed in a 20 mm diameter graphite die with thin graphite foil as an electric conductive support. Afterward, a load of 9 kN was applied at the beginning of the heating cycle, then a heating rate in the sintering temperature range of 100 °C/min was imposed. In order to avoid grain coarsening of the microstructure of the sintered specimen, the process was conducted below the γ prime temperature, which is about 1140 °C (1413 K) [24–26]. After 10 min of dwell time at the sintering temperature, the ram pressure was released, and the specimen was allowed to cool in the furnace. A set of 7 coupons were obtained at a temperature range of 800 °C to 1100 °C. In turn, each sintered coupon was polished with 1000-grade SiC paper to analyse the microstructure and mechanical properties of the developed coupons. Table 1 summarises the conditions of the performed SPS processes to obtain the set of sintered coupons (named: A, B, C, D, E, F, and G). Archimedes' principle was used to assess the porosity of each sintered coupon. To analyse possible transformation phases of the as-received Diamalloy powders, a differential scanning calorimetry apparatus (DSC) SDT Q600 V20.9 Build 20 was employed with the following conditions: 1 Ramp 50.00 °C/min to 600.00 °C and 2 Ramp 10.00 °C/min to 1300.00 °C, atmosphere air, and alumina crucible. Vickers hardness measures were carried out using a Mitutoyo AVK-C2 Akashi apparatus. In addition, three-point bending tests were performed following the ASTM E-290-22 [27] standard test method at 23 °C using a computer-controlled mechanical

tester and UH-30A Shimadzu machine (Kyoto, Japan, 100 kN to 1000 kN) to provide a cross-sectional coupon surface analysis.

Table 1. Temperature and load applied in each SPS process.

Sample	Temperature (°C)	Heating Rate (°C/min)	Axial Load (GPa)
A	800	50	9
B	850	100	9
C	900	50	9
D	950	100	9
E	1000	100	9
F	1050	100	9
G	1100	100	9

3. Results and Discussion

3.1. Densification

Figure 1 shows the features of the Diamalloy 3001 powders from the SULZER manufacturer (Winterthur, Switzerland). Figure 1a shows that the powder is composed of a spheric morphology with a distribution size in the range of 10 µm to 40 µm, which is also shown in the plot in Figure 1b. Figure 1c shows a higher magnification image of the spherical powders. Figure 1d shows an image of the microstructural characteristics of the Diamalloy 3001 powder, which is comprised of a smooth surface with dendritic growth observed on the surface.

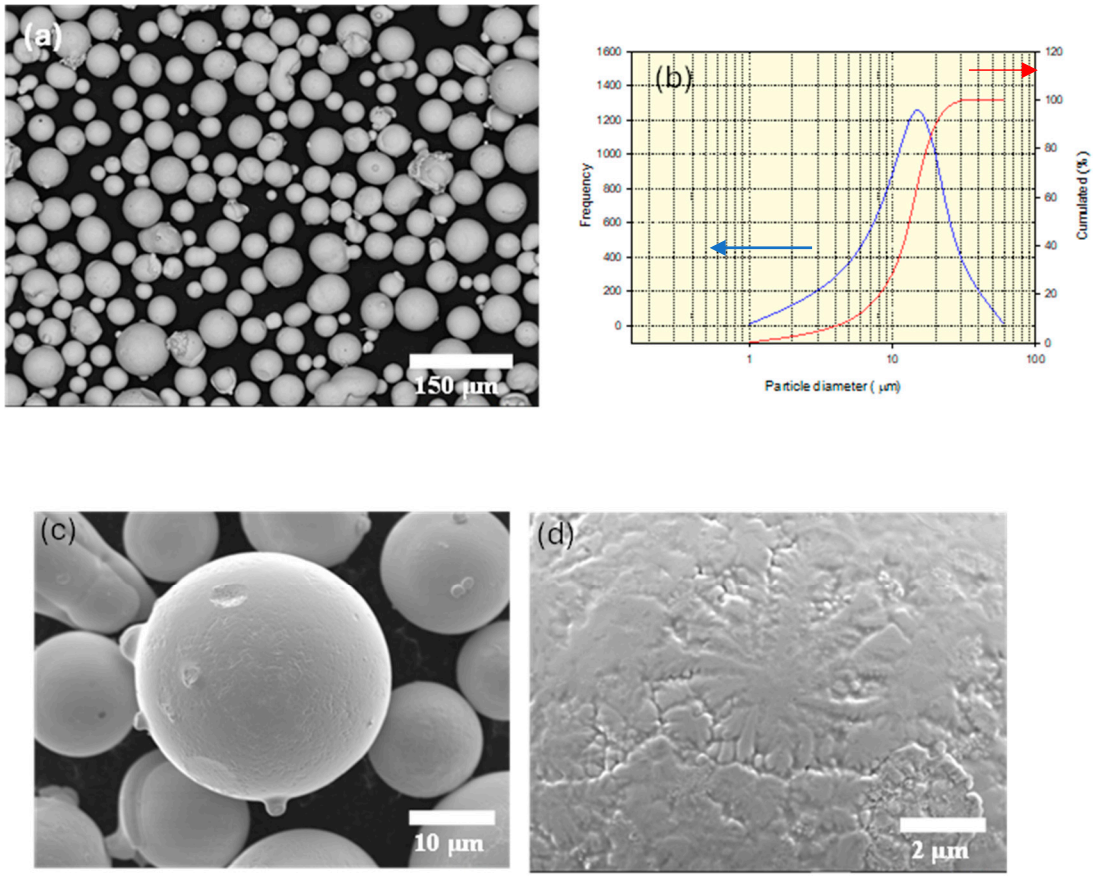

Figure 1. (**a**) Diamalloy Co-based alloy powder as received from the SULZER manufacturer, (**b**) plot of the size distribution of the powder, (**c**) close-up view of the spherical morphology of the powder, and (**d**) powder microstructure composes of dendritic growths of a size around 4 µm.

The spark plasma sintering behaviour of the Co-based alloy powder is shown in Figure 2. The set of different temperatures applied in the SPS process, which is a function of the time employed for the densification of powders, is shown in Figure 2a. As is observed in the plot, the temperature increased linearly as a function of time to reach the desired temperature for each different sample, as described in Table 1.

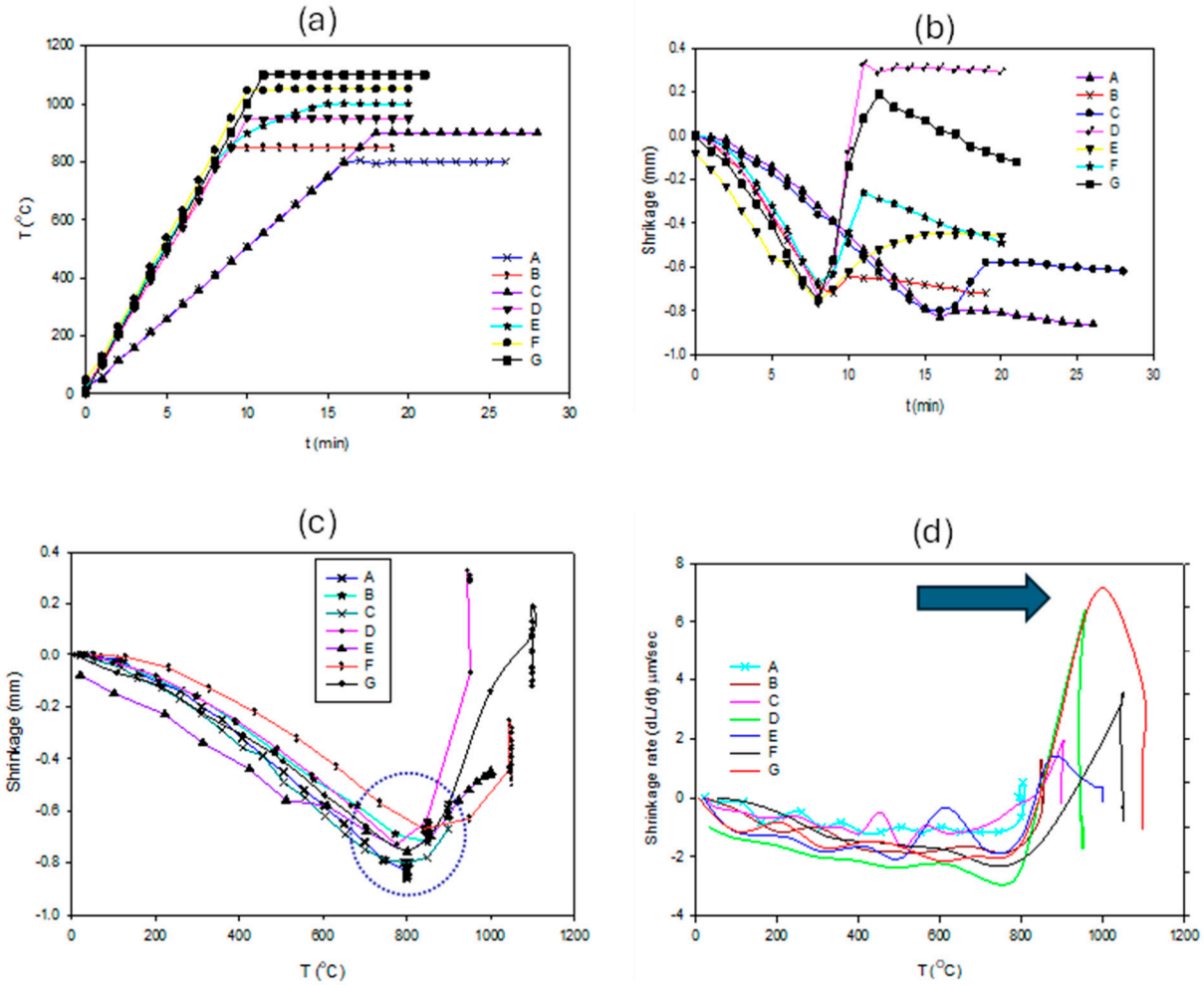

Figure 2. Spark plasma sintering behaviour of Diamalloy Co-based alloy powder: (**a**) temperature vs. time, (**b**) shrinkage vs. time, (**c**) shrinkage vs. temperature, and (**d**) shrinkage rate vs. temperature.

Figure 2b shows the shrinkage behaviour as a function of time for each sample and defined temperature. From this plot, it can be observed that shrinkage values varied with the time increment. Thus, at the beginning of sintering, the shrinkage values decreased until a minimum value of around −0.6 mm for sample C and a maximum value of 0.4 mm for sample D were reached. In the literature, many research works have reported graphs of the shrinkage behaviour for different ceramics and alloys [21,28,29]. In such works, it was observed that the work temperature significantly influenced the shrinkage, which had a relationship with the degree of densification [21]. Figure 2c shows a plot of the shrinkage for each sample as a function of the applied temperature; it was observed that shrinkage values presented a slight variation for each sintering temperature, and a minimum shrinkage value was identified (blue dotted circle).

Thus, the minimum shrinkage value was found at a temperature of 800 °C, which would correspond to each sintered coupon. This last condition suggests that the parameter that controls the sintering is the maximum temperature applied during the SPS process. In the same sense, for samples A and C, where the lowest heating rate (50 °C/min) was applied to reach the designated temperature, the minimum shrinkage value was similar to

that of highest heating rate (100 °C/min), as observed in Figure 2c. Therefore, the heating rate did not influence the densification of the powder. To elucidate the dwell time effect during the sintering process in isotherm conditions, the shrinkage rate (densification rate) is plotted as a function of the sintering temperature in Figure 2d. Again, it was observed that the shrinkage rate incremented with the increase in the sintering temperature; thus, with an increment of 50 °C from 1050 to 1100 °C, the shrinkage rate reached a maximum value (sample G, depicted by blue arrow) of around 7 µm/s. This value would signify a higher densification stage accomplished for the Co-based alloy powder. In other words, this high shrinkage rate value for sample G was achieved in about 10 min; afterward, the shrinkage rate value decreased dramatically to 0.2 µm/s in about 20 min, and then it finally dropped. Therefore, this higher shrinkage rate was associated with reaching the maximum densification during SPS conditions for the powder. It was observed that only at 1100 °C was a maximum shrinkage value reached, which mains the microstructural evolutionary end for the sintering of the powders, and the existence of a sintering main mechanism, is possibly evidenced by this behaviour.

The DCS analysis of the as-received Diamalloy powder evidences the existence of possible transformation phases at temperatures of 592, 890, and 1030 °C as indicated by arrows in Figure 3. However, only the last two temperatures showed a relationship with both the minimum shrinkage and maximum shrinkage rates previously identified in Figure 2c,d, respectively.

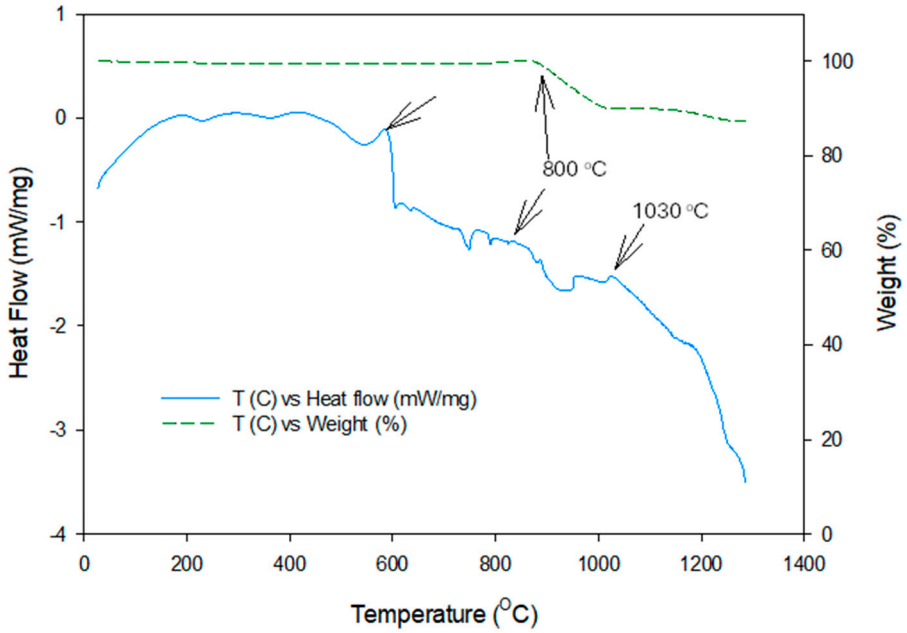

Figure 3. DCS analysis of the Diamalloy Co-based alloy powder.

3.2. Microstructure

Several mechanisms can be induced by the high-intensity electrical current during the SPS process: (i) arcs and plasma generation between powder particles, (ii) dielectric breakdown of the oxide layers at the surface of the powder particles, (iii) local overheating due to a current density increase at the contact between powder particles, and (iv) activation of electromigration and electroplasticity [11–18].

In order to evaluate the densification quality and the chemical composition of the sintered coupons manufactured by the SPS process, in this section, the effect of temperature on the microstructure during the sintering process of Co-based alloy powders is analyzed. Figure 4 shows micrographs of the microstructure of the coupons sintered in the following temperature range: from 800 °C to 1000 °C. A poor-quality densification for coupon A is shown in Figure 4a; here, the microstructure was composed of a morphology likes to

that of the as-received powders, which was preserved. Figure 4b shows a micrograph of the sintered coupon B, which clearly shows better densification; thus, the porosity was decreased, as observed by the dark regions in the figure. The spheroidal morphology of the large powders seemed to be properly maintained. The quantitative EDS analysis clearly shows that a high Cobalt base element was predominant in the material matrix of the sintered sample. Figure 4c shows a micrograph of coupon C sintered at a temperature of 900 °C; the microstructure was formed with a relatively low porosity. It is worth noting that an increment in the heating ramp did not promote a change in the development of the microstructure, as was shown by the shrinkage rate value (Figure 4d). Moreover, it is possible to observe the development of small zones marked by a grey colour. Figure 4d shows a micrograph of coupon D sintered at a temperature of 950 °C, where an increment of 50 °C of temperature improved the densification. Nonetheless, the microstructure still appears to have formed by morphology like-spherical powder, though an increase in the size of the light grey zones was observed, which was possibly caused by the sintering of the small powder with a high surface energy.

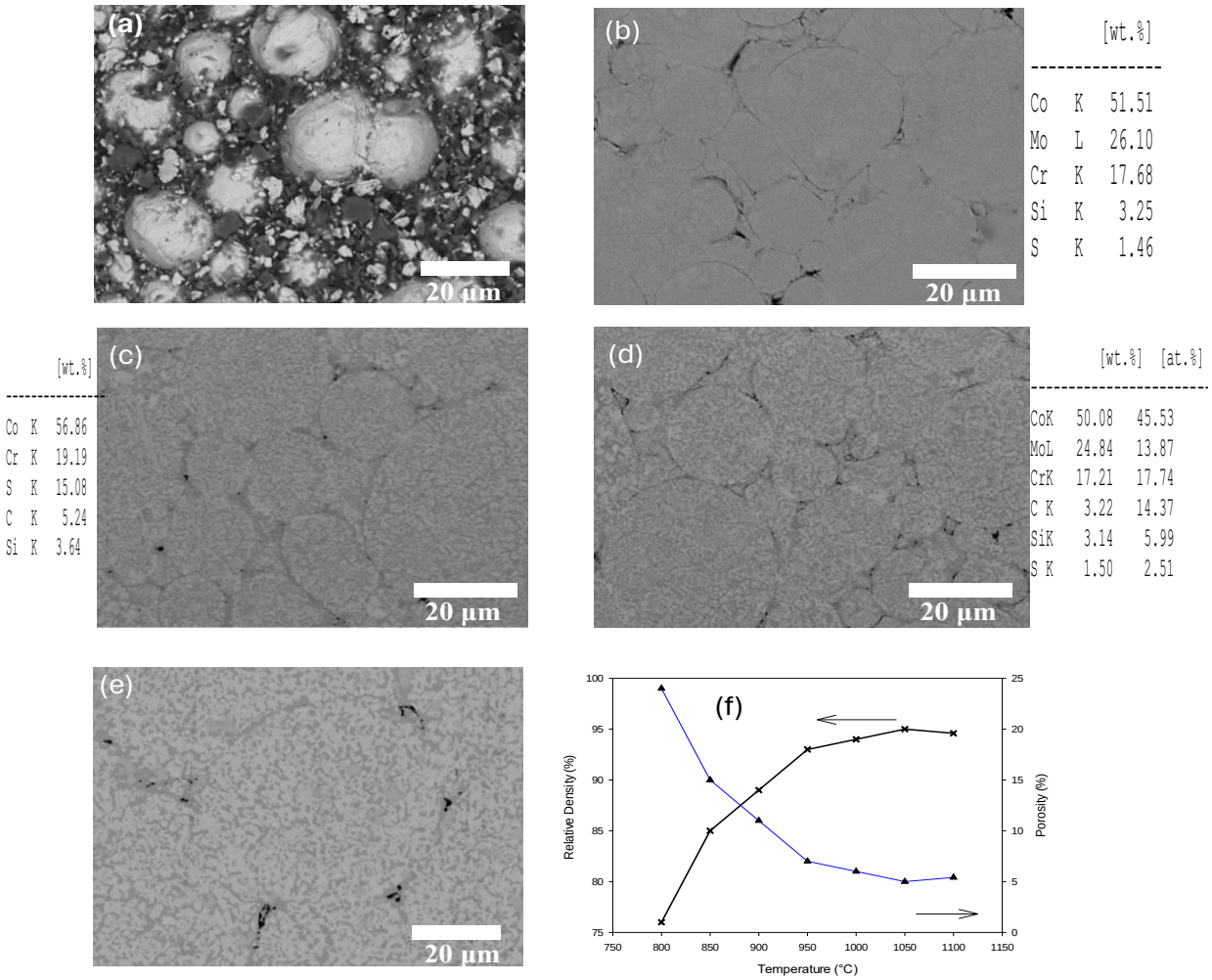

Figure 4. Micrographs of sintered coupons for samples A to E: (**a**) 800 °C, (**b**) 850 °C, (**c**) 900 °C, (**d**) 950 °C, (**e**) 1000 °C, and (**f**) plot of relative density and porosity vs. temperature.

Figure 4 also shows a micrograph of the microstructure of the coupon sintered at a temperature of 1000 °C. The microstructure is comprised of zones marked by a light grey and grey colour. Once again, the initial features seem to still be preserved, though the diminution of small pores in the sintered matrix was noted, as observed in Figure 4e. Accordingly, Figure 4f shows a plot of the relative density reached for each sintered coupon

as a function of the temperature in a range of 800 °C to 1100 °C. This plot clearly shows an increment in the relative density when an increment in the sintering temperature was applied. Accordingly, a relative density of 95 percent was achieved for the coupon sintered at 1100 °C.

Figure 5a shows micrographs of the microstructure of the coupon sintered at a temperature of 1050 °C. The presence of small or even no porosity can be observed in the sintered coupon. The microstructure was constituted by a fine morphology as depicted by zones in light grey and white colours. An EDS mapping analysis of the sintered coupon shows that rich zones are comprised of Co, Mo, Si, and Cr elements (Figure 5b). In this condition, the microstructure is comprised of fine phases distributed homogeneously in the Co matrix; they could be Co-Cr, Mo-Si, and rich Mo, as shown in Figure 5a. The development of a fine microstructure suggests the presence of a stage promoted by simple surface diffusion, which in turn proves the volume reduction by the reduction in the porosity. Moreover, this indicates the presence of a main sintering mechanism caused by surface diffusion when a sintering temperature of 1050 °C is imposed.

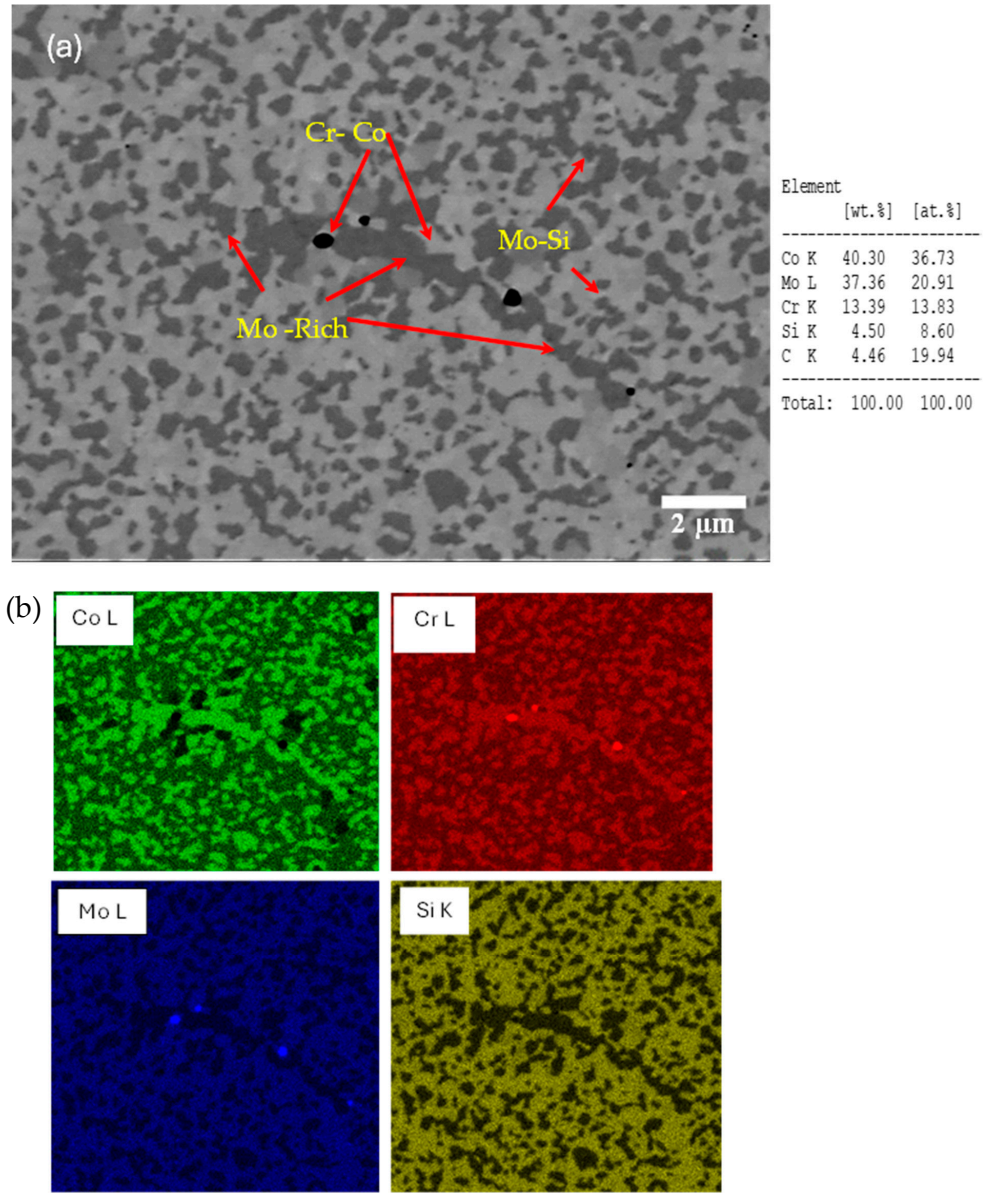

Figure 5. (**a**) Microstructure of the coupon sintered at 1050 °C and (**b**) EDS map analysis of Co, Cr, Si, and Mo chemical elements.

Lastly, Figure 6 shows the developed microstructure of the coupon sintered at a temperature of 1100 °C. The microstructure is clearly constituted by the formation of zones well-identified by grey and white colours, as seen in Figure 6a,b, respectively. Moreover, the presence of porosity was not observed, and plaques-like morphologies ranging from 2 to 4 µm were distributed homogeneously in the sintered matrix. To elucidate the chemical composition of such morphologies, Figure 6 shows the EDS maps of the sintered G coupon, where zones rich in Mo-Si, Co, and Cr elements were identified.

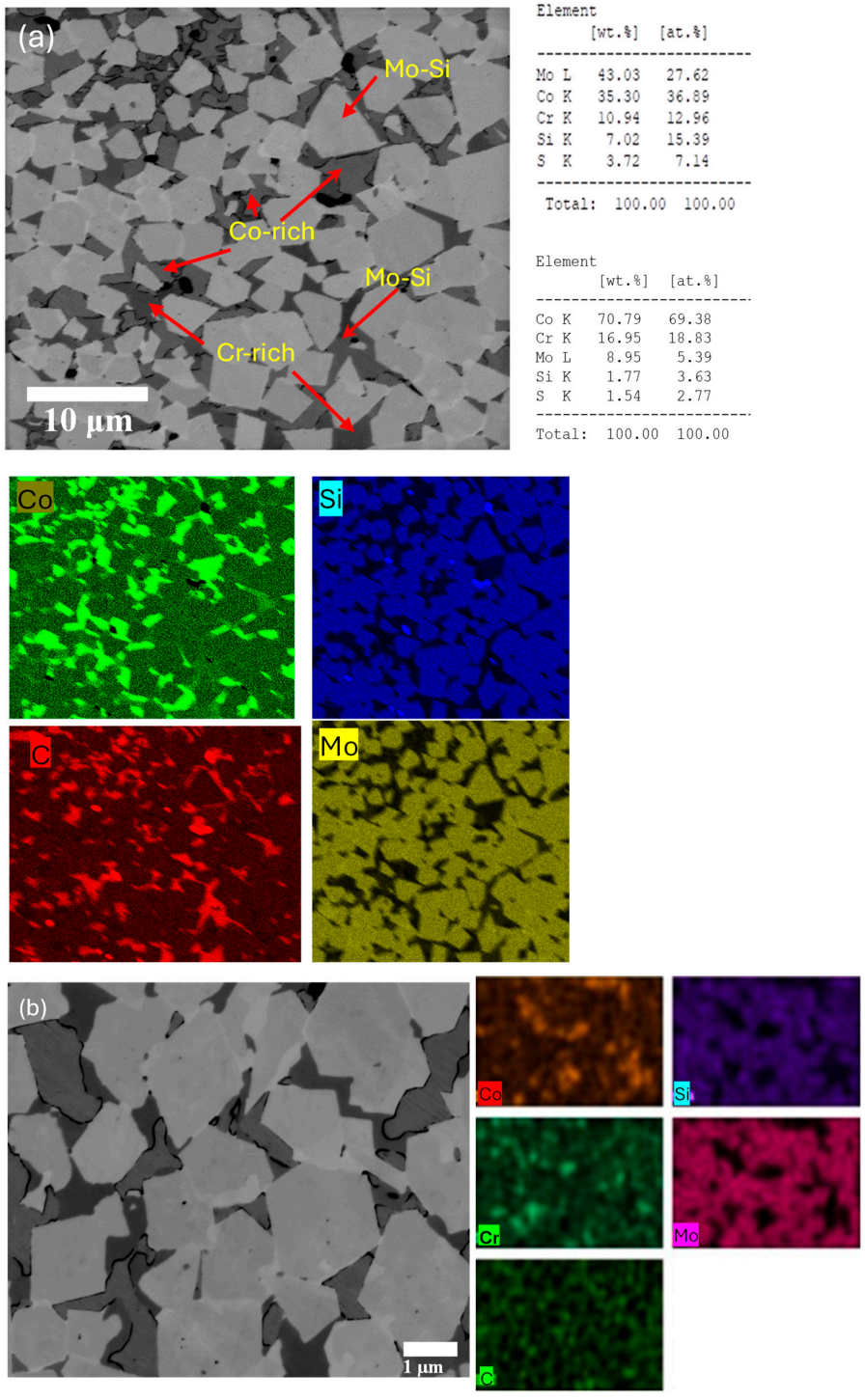

Figure 6. Micrographs of the coupon sintered at a temperature of 1100 °C: (**a**) microstructure and quantitative analysis and (**b**) microstructure at a higher magnification and map of the EDS analysis of the sintered coupon at a temperature of 1100 °C.

Therefore, at this temperature, the microstructure was comprised of a rich Mo-Si phase homogeneously dispersed in the Co matrix. Hence, the controlled temperature condition during the sintering process allowed for densified coupons comprised of Mo_6Co_6 and Mo-Si phases with a plaque-like morphology of 4 μm in size. These last phases have been crystallography reported in the literature [24–26].

XRD analysis was carried out to identify the crystalline structure of the sintered coupons in order to show cobalt phases in the material matrix sintered at a temperature range of 800 to 1100 °C, as observed in Figure 7.

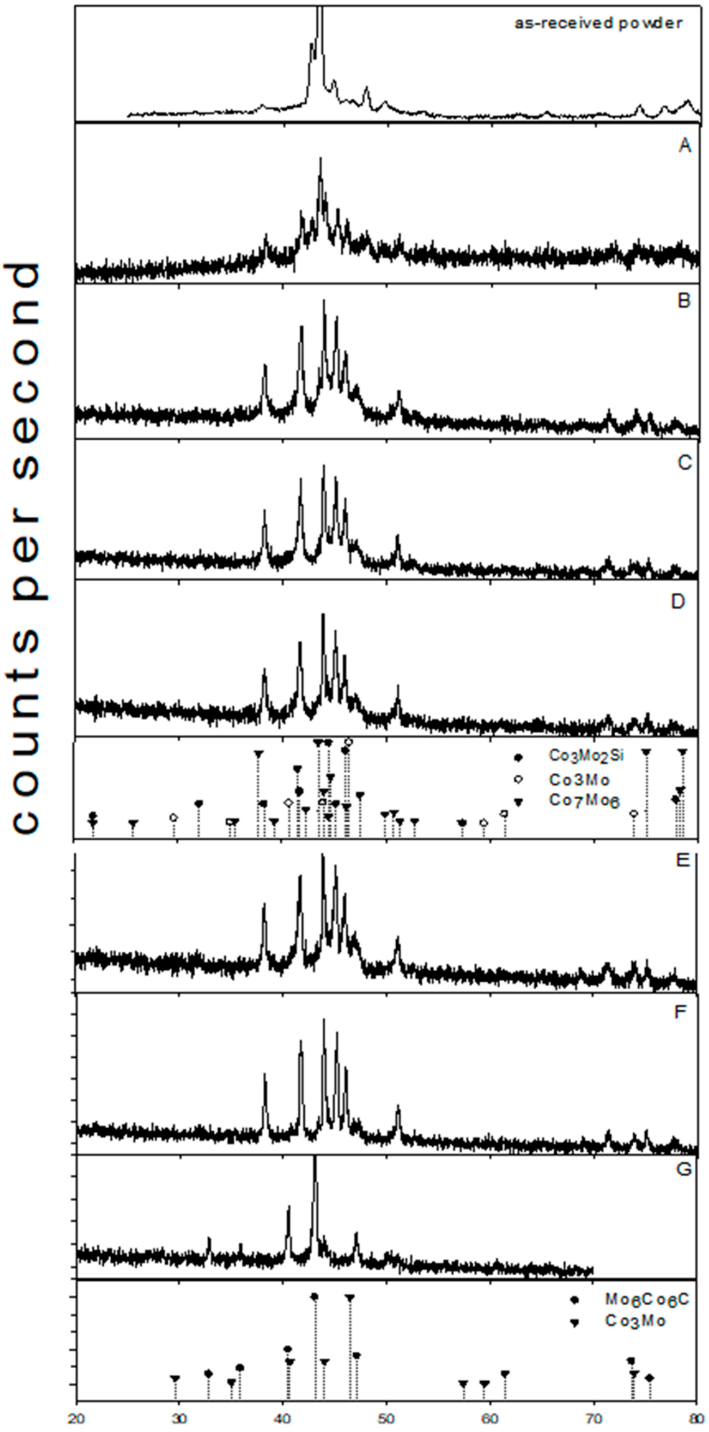

Figure 7. XRD analysis of each sintered coupon at a temperature range of 800 °C to 1100 °C: samples (**A**–**G**).

The experimental diffractograms for coupons A–F corresponded to ISCD patterns indexed with a hexagonal structure, as follows: Co_7Mo_6 phase 2310288, Co_3Mo_2Si 030-0449, and Co_3Mo 2310283 with parameters a: 4.7 (Å) and c: 7.67 (Å). It worth noting that these last laves phases have been reported in the literature for the Co-Cr-Mo-Si system [25], though they used a mixture melted in an arc furnace under a high-purity argon atmosphere for the synthesis of that matrix. It was observed that these phases were clearly preserved during sintering at a temperature range of 800 °C to 1050 °C, as seen in Figure 7. Moreover, these phases corresponded to the as-received Co-based alloy powder. Therefore, the SPS process did not modify the crystalline structure of the sintered coupons in the whole temperature range; moreover, SPS conditions preserved the fine microstructure of the as-received powder.

However, at a sintering temperature of 1100 °C, the XRD analysis shows the presence of phases that correspond to indexed ICSD patterns: Co_3Mo 2310283 and Mo_6Co_6C 03-065-8115. The presence of these phases implies the transformation of the phases under SPS conditions; moreover, it suggests the development of a second stage of sintering by simple volume diffusion. It worth noting the formation of a phase rich in the C element, which would imply a reaction with the Cobalt matrix by the formation of carbides. Several works have reported the presence of adsorption or reaction due to the C evaporation from the graphite die when sintering reaches up the 700 °C [30–32]. Hence, it can be observed that the formation of the last phases is associated with an important increment in the hardness values of the sintered coupons.

In summary, the results show that the applied temperature and the dwell time in the SPS conditions allowed for the improved densification of the Diamalloy 3001 alloy powder. Therefore, it can be concluded that the temperature parameter played a vital role in the development of the microstructure.

3.3. Mechanical Properties

In this section, micro-hardness tests were carried out to measure the hardness properties of all coupons sintered through the SPS process of Co-based Diamalloy 3001 powders. It is important to mention that before performing the tests, the microhardness test machine was verified to be recently calibrated according to ISO-6507 Standards [33].

In order to perform the Vickers hardness tests, five testing points were defined on each sample. Then, the standard deviation of the obtained Vickers hardness values was determined. In the Vickers micro hardness testing, a mass of two kilograms was applied to create the diamond mark characteristic. The tests were carried out following the recommendations reported in the literature [33,34]. Figure 8a shows a plot of the measured Vickers hardness values obtained from coupons A to G; thus, hardness values increased with the increment in the sintering temperature. However, it was observed that sample G presented higher Vickers hardness values compared to the other SPS sintering temperatures. This last Vicker hardness value of 14 GPa is quasi similar to that reported in the literature [3–7]; here, the last values were attributed to the presence of a Co_6Mo_6C phase formed at a temperature of 1100 °C, as was previously indicated by the XRD results. Figure 8b,c shows the Vickers diamond indentation marks from sample G. These marks present features of a slight strained structure, which can be attributed to the brittle mechanical behaviour of the material.

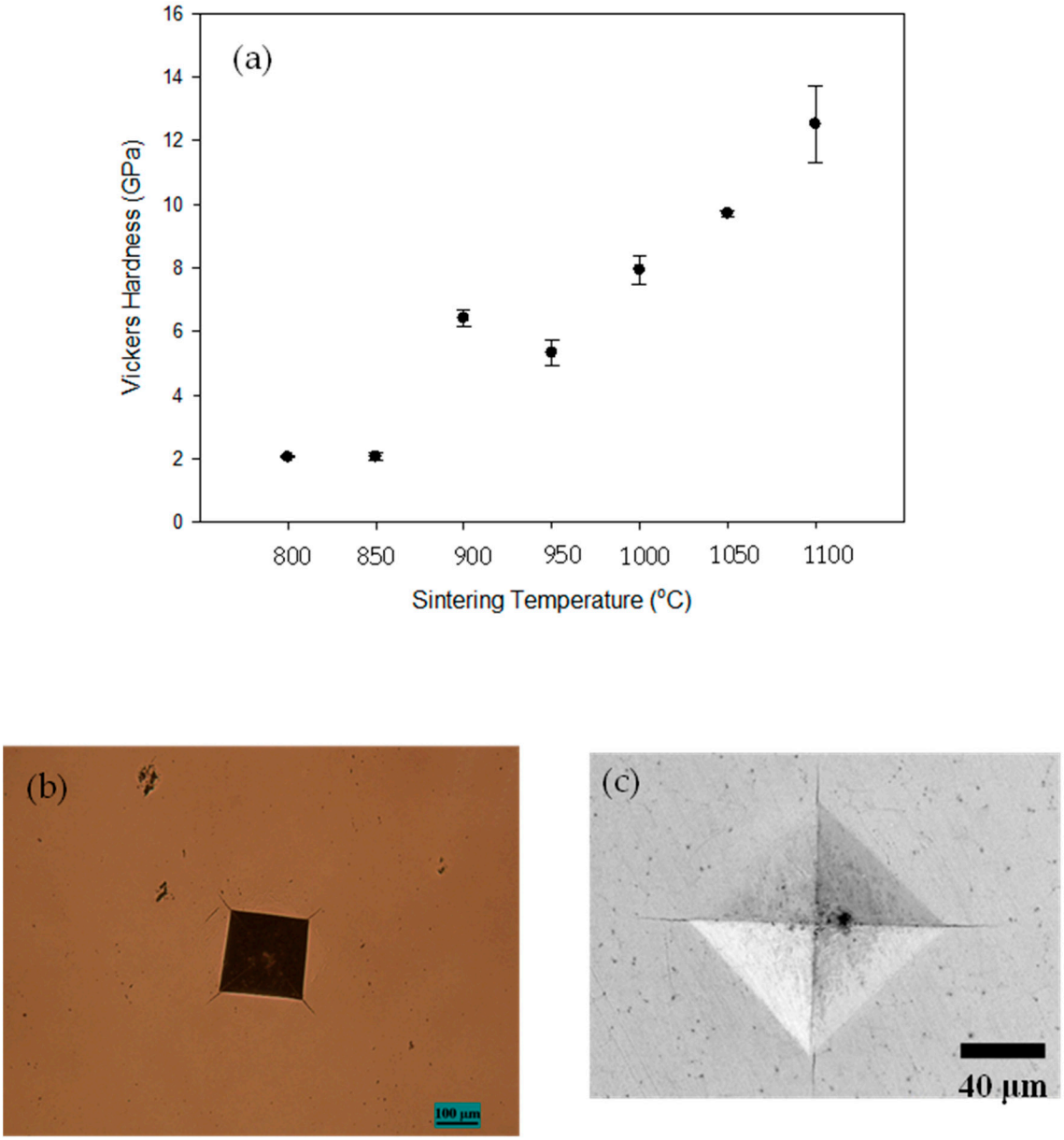

Figure 8. (**a**) Plot of Vickers hardness vs. sintering temperature for the different sintered coupons and (**b**,**c**) optical and micrograph images from indentation marks of sintered coupon at 1100 °C.

Three-point bending tests were carried out in order to provide cross-sectional sintered coupon surface analysis. Figure 9 shows the resultant fracture surface of the sintered coupons after the bending test. Figure 9a shows a cross-section of sintered coupon B, where powder–powder bonding was clearly observed; moreover, a spalling surface powder caused by bending test was observed. Figure 9b also shows sintered coupon C after the bending test. Here, better powder–powder bonding was observed. It is worth noting that the fine powder microstructure was still preserved after a sintering temperature of 900 °C. Figure 9c shows the fracture surface of sintered coupon G. From this, densification of the whole powder was observed; moreover, the microstructure shows a fracture surface correlated with the degree of densification of the coupon sintered at 1100 °C. In summary, the micrographs show a fracture surface typical of brittle materials with morphologies like a flat face.

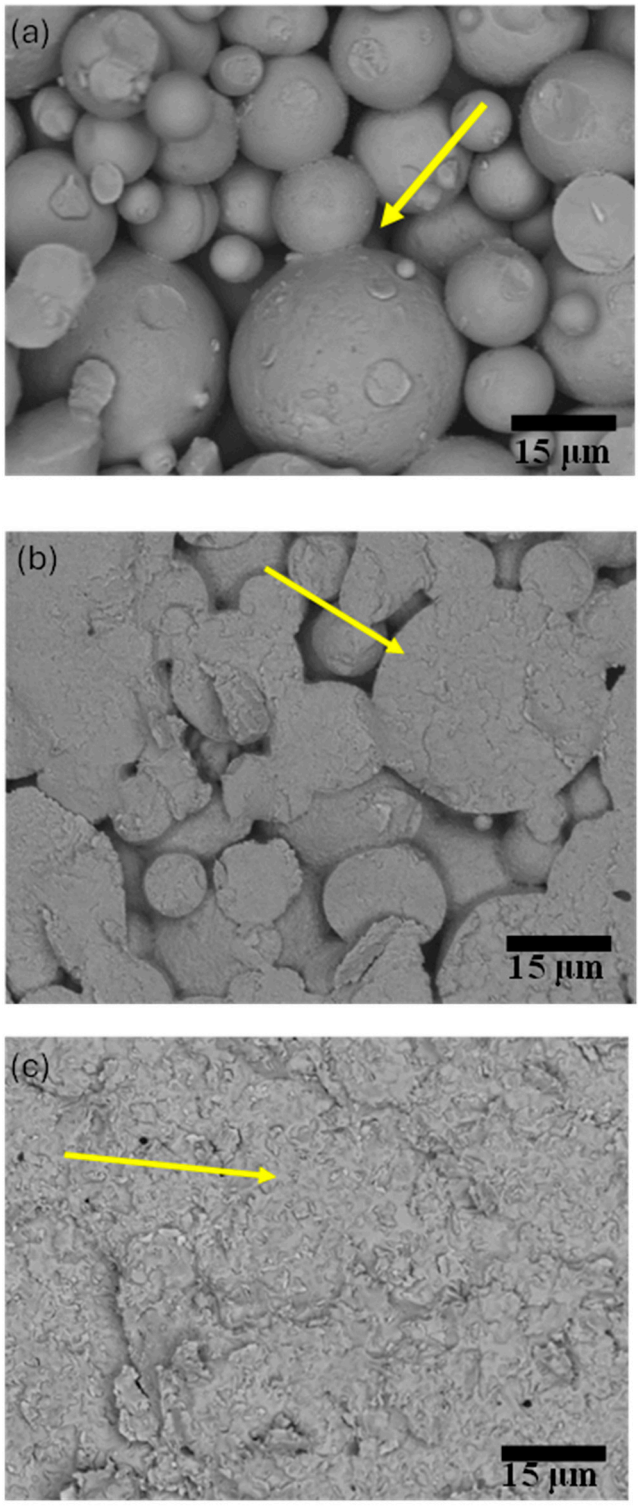

Figure 9. Surface fracture resultant of sintered coupons after bending test: (**a**) B sample powder-powder bonding (yellow arrow), (**b**) C sample, dendritic microstructure (yellow arrow), and (**c**) G sample densified microstructure (yellow arrow), respectively.

4. Conclusions

The purpose of the present work was to study the sintering of Diamalloy Co-based alloy powders by the SPS process. The obtained shrinkage data were plotted to show the dependence with the sintering temperature in the range of 800 °C to 1100 °C. The resultant maximum shrinkage rate corresponded to an obtained microstructure by gradual

increments of 50 °C of the sintering temperature. The densified microstructure sintered at a temperature of 1100 °C constituted the presence of plaque-like morphologies and was comprised of laves phases rich in the Co element. High hardness values in the range of 12 to 14 GPa were attributed to the development of the Co_6Mo_6C lave phase, which was homogeneously distributed in the matrix of the alloy. The controlled increment of 50 °C of the sintering temperature allowed for the microstructural evolution of the Co-based alloy powders. An increase in the temperature allowed the powder particle bonding, as was observed in the micrographs. Also, the implication of two sintering mechanisms was proposed for the densification of the Co alloy powder. Thus, at the beginning of sintering, a surface diffusion mechanism was present at the temperature range of 800 to 1050 °C; afterward, the volume diffusion mechanism was present up to 1100 °C. The above data of the densification kinetic provide information for the designing of full parts and of complicated shapes using cobalt alloys.

Author Contributions: Conceptualization, F.J.-L., M.G.-H. and R.C.-M.; methodology, F.J.-L. and M.L.C.-J.; investigation, F.J.-L. and Á.d.J.M.-R.; writing—original draft preparation, F.J.-L. and R.C.-M.; writing—review and editing, Á.d.J.M.-R. All authors have read and agreed to the published version of the manuscript.

Funding: This research received no external funding.

Institutional Review Board Statement: Not applicable.

Informed Consent Statement: Not applicable.

Data Availability Statement: Data sharing is not applicable to this article.

Acknowledgments: The authors acknowledge to Comisión de Fomento a las Actividades Académicas, Estimulo al desempeño de los Investigadores, Sistema Nacional de Investigadores, Consejo Nacional de Humanidades, Ciencia y Tecnología, and R. Cuamatzi-Meléndez to México postdoctoral stays 2022 (3) No. I1200/320/2022 for the provided support. Special acknowledgment to Ricardo Escalona G. for the coupons preparation.

Conflicts of Interest: The authors declare no conflicts of interest.

References

1. American Bureau of Shipping. ABS Guide for Classification and Certification of Subsea Production Systems Equipment and Components. 2017. Available online: www.eagle.org (accessed on 1 April 2023).
2. Iannuzzi, M.; Barnoush, A.; Johnsen, R. Materials and corrosion trends in offshore and subsea oil and gas pro-duction. *NPJ Mater Degrad.* **2017**, *1*, 2. [CrossRef]
3. An, X.; Li, Y.; Ni, S.; Wang, Z.; Song, M. Microstructural and hardness evolutions of a cold-rolled cobalt. *Mater. Sci. Eng. A* **2021**, *803*, 140712. [CrossRef]
4. Khatavkar, N.; Swetlana, S.; Singh, A.K. Accelerated prediction of Vickers hardness of Co- and Ni-based superalloys from microstructure and composition using advanced image processing techniques and machine learning. *Acta Mater.* **2020**, *196*, 295–303. [CrossRef]
5. Cai, J.; Feng, K.; Liu, Y. Studies towards activation of cobalt in W-Mo-Cu alloy sintered via large current electric field. *Int. J. Refract. Met. Hard Mater.* **2023**, *117*, 106406. [CrossRef]
6. Moharrami, N.; Langton, D.; Sayginer, O.; Bull, S. Why does titanium alloy wear cobalt chrome alloy despite lower bulk hardness: A nanoindentation study? *Thin Solid Film.* **2013**, *549*, 79–86. [CrossRef]
7. Şahin, M.; Ünalan, F.; Mutlu, I. Corrosion, ion release, and surface hardness of Ti-6Al-4V and cobalt-chromium alloys produced by CAD-CAM milling and laser sintering. *J. Prosthet. Dent.* **2022**, *128*, 529.e1–529.e10. [CrossRef]
8. Kang, J.-S.L. *Sintering Densification, Grain Growth & Microstructure*, 1st ed.; Elsevier: Oxford, UK, 2004; ISBN 9780080493077.
9. Nguyen, V.M.; Khanna, R.; Konyukhov, Y.; Nguyen, T.H.; Burmistrov, I.; Levina, V.; Golov, I.; Karunakaran, G. Spark plasma sintering of cobalt powders in conjunction with high energy mechanical treatment and nano-modification. *Processes* **2020**, *8*, 627. [CrossRef]
10. Cinert, J. *Study of Mechanisms of the Spark Plasma Sintering Technique*; Czech Technical University in Prague: Prague, Czechia, 2018.
11. Voisin, T.; Monchoux, J.P.; Durand, L.; Karnatak, N.; Thomas, M.; Couret, A. An innovative way to produce-TiAl blades: Spark plasma sintering. *Adv. Eng. Mater.* **2015**, *17*, 1408–1413. [CrossRef]
12. Manière, C.; Nigito, E.; Durand, L.; Weibel, A.; Beynet, Y.; Estournès, C. Spark plasma sintering and complex shapes: The deformed interfaces approach. *Powder Tech.* **2017**, *320*, 340–345. [CrossRef]

13. Voisin, T.; Monchoux, J.P.; Couret, A. Near-net shaping of titanium-aluminum jet engine turbine blades by SPS. In *Spark Plasma Sintering of Materials*; Cavaliere, P., Ed.; Springer: Cham, Switzerland, 2019; pp. 713–737.
14. Tokita, M. The potential of spark plasma sintering (SPS) method for the fabrication on an industrial scale of functionally graded materials. *Adv. Sci. Tech.* **2010**, *63*, 322–331.
15. Monchoux, J.-P.; Couret, A.; Durand, L.; Voisin, T.; Trzaska, Z.; Thomas, M. Elaboration of Metallic Materials by SPS: Processing, Microstructures, Properties, and Shaping. *Metals* **2021**, *11*, 322. [CrossRef]
16. Munir, Z.A.; Ohyanagi, M. Perspectives on the spark plasma sintering process. *J. Mater. Sci.* **2021**, *56*, 1–15. [CrossRef]
17. Cavaliere, P. *Spark Plasma Sintering of Materials: Advances in Processing and Applications*; Springer: Berlin/Heidelberg, Germany, 2019. [CrossRef]
18. Hu, Z.Y.; Zhang, Z.H.; Cheng, X.W.; Wang, F.C.; Zhang, Y.F.; Li, S.L. A review of multiphysical fields induced phenomena and effects in spark plasma sintering: Fundamentals and applications. *Mater. Des.* **2020**, *191*, 108662. [CrossRef]
19. Dobrzański, L.A.; Dołżańska, B.; Gołombek, K.; Matula, G. Characteristics of structure and properties of a sintered graded tool materials with cobalt matrix. *Arch. Mater. Sci. Eng.* **2011**, *47*, 69–76.
20. Lima, F.T.C.; Bobrovinitchii, G.S.; Filgueira, M. Study of the Diamond 5%wt-Cobalt Sintering under the HPHT Lowest Limit. *Mater. Sci. Forum* **2005**, *498–499*, 225–230. [CrossRef]
21. Buravleva, A.A.; Fedorets, A.N.; Vornovskikh, A.A.; Ognev, A.V.; Nepomnyushchaya, V.A.; Sakhnevich, V.N.; Lembikov, A.O.; Kornakova, Z.E.; Kapustina, O.V.; Tarabanova, A.E.; et al. Spark plasma sintering of WC-based 10wt%Co hard alloy: A study of sintering kinetics and solid-phase processes. *Materials* **2022**, *15*, 1091. [CrossRef] [PubMed]
22. Fanicchia, F.; Maeder, X.; Ast, J.; Taylor, A.; Guo, Y.; Polyakov, M.; Michler, J.; Axinte, D. Residual stress and adhesion of thermal spray coatings: Microscopic view by solidification and crystallisation analysis in the epitaxial CoNiCrAlY single splat. *Mater. Des.* **2018**, *153*, 36–46. [CrossRef]
23. Gao, Y. Characterization and Mechanical Properties for Diamalloy 3001 and Diamalloy 3002NS Thermally Sprayed Coatings. Master's Thesis, McGill University, Montreal, QC, Canada, 2020.
24. Kamardan, M.G.; Zaidi, N.H.; Dalimin, M.N.; Zaidi, A.M.; Jamaludin, S.B.; Jamil, M.M. The sintering temperature effect on the shrinkage behavior of cobalt chromium alloy. *Am. J. Appl. Sci.* **2010**, *7*, 1443–1448. [CrossRef]
25. Jiang, S.; Yin, F.; Zhang, M.; Zhao, M.; Li, Z. 800 OC isothermal section of the Co–Cr–Mo–Si qua-ternary system. *Int. J. Mater. Res.* **2014**, *105*, 12. [CrossRef]
26. Khouzani, M.K.; Bahrami, A.; Mehr, M.Y. Spark plasma sintering of Stellite®-6 superalloy. *J. Alloys Compd.* **2019**, *782*, 461–468. [CrossRef]
27. *E290 – 22*; Standard Test Methods for Bend Testing of Material for Ductility. ASTM International: West Conshohocken, PA, USA, 2022. [CrossRef]
28. Rajan, K. Thermodynamic assessment of heat treatments for a Co-Cr-Mo alloy. *J. Mater. Sci.* **1983**, *18*, 257–264. [CrossRef]
29. Zhao, J.-C. Phase Diagram Determination Using Diffusion Multiples. In *Methods for Phase Diagram Determination*; Elsevier Science Ltd.: Amsterdam, The Netherlands, 2007; Chapter Seven. [CrossRef]
30. He, Z.; Yuan, H.; Glasscock, J.A.; Chatzichristodoulou, C.; Phair, J.W.; Kaiser, A.; Ramousse, S. Densification and grain growth during early-stage sintering of $Ce_{0.9}Gd_{0.1}O_{1.95-\delta}$ in a reducing atmosphere. *Acta Mater.* **2010**, *58*, 3860–3866. [CrossRef]
31. Esposito, V.; Ni, D.W.; He, Z.; Zhang, W.; Prasad, A.S.; Glasscock, J.A.; Chatzichristodoulou, C.; Ramousse, S.; Kaiser, A. Enhanced mass diffusion phenomena in highly defective doped ceria. *Acta Mater.* **2013**, *61*, 6290–6300. [CrossRef]
32. Klemens, P.G. Phonon scattering by oxygen vacancies in ceramics. *Phys. B Condens. Matter* **1999**, *263–264*, 102–104. [CrossRef]
33. *ISO 6507-1*; Metallic Materials-Vickers Hardness Test—Part 1: Test Method. International Standard. ISO: Geneva, Switzerland, 1997.
34. *ASTM E 92–82*; Standard Test Method for Vickers Hardness of Metallic Materials. American Society for Testing and Material: West Conshohocken, PA, USA, 1997; pp. 1–10.